JOURNAL OF MATERIALS SCIENCE **38** (2003) 4385–4391

Simulation of dendritic growth in the platform region of single crystal superalloy turbine blades

W. WANG
Department of Materials, Imperial College, London SW7 2BP, UK

A. KERMANPUR
Department of Materials, Imperial College, London SW7 2BP, UK;
Department of Materials Engineering, Isfahan University of Technology, Isfahan 84156, Iran

P. D. LEE, M. MCLEAN
Department of Materials, Imperial College, London SW7 2BP, UK
E-mail: p.d.lee@ic.ac.uk

A cellular automaton model of the solid-liquid interface, combined with a finite difference computation of solute diffusion has been developed to simulate single crystal solidification in molds with step changes in geometry. Simulations were carried out for columnar dendrites passing from the narrow airfoil region of a blade into the platform region, which has an increased cross-sectional area. Different shapes of isotherms moving at a constant velocity were considered in the simulations. The change in mold geometry leads to a significant increase in the undercooling in front of the dendrite tips as they spread around the mold corner. The model was applied to geometries investigated by prior authors, correctly predicting the formation of a ⟨001⟩ to ⟨010⟩ boundary observed experimentally.

1. Introduction

Single crystal (SX) nickel-base superalloys are the current state-of-the-art for producing gas turbine blades that satisfy the stringent quality required to ensure mechanical integrity at the high operating temperatures in modern engines. The final casting integrity of these parts, which are produced by a unidirectional solidification process, depends upon their microstructures and inherent defects [1]. Many types of performance-limiting crystal defects, such as freckles, stray grains, recrystallized grains, low-angle boundaries and microporosity can occur in a SX part. Some of these defects are difficult to eliminate in large, complex shaped blades. The mechanisms for formation of these defects are known in a general sense and some progress has been achieved in identifying their origins and quantifying their causes [2–4]. Given the cost constraints associated with design and manufacture of the SX parts, casting designers have become increasingly reliant on modeling and simulation of the casting process in order to produce defect-free components.

So far extensive macroscopic numerical simulations have been performed based on thermal finite element analysis, correlating the macroscopic solidification conditions (e.g., thermal gradient, G, solidification rate, R, cooling rate and local solidification time) to the microstructures produced and the likelihood of defects being found in SX castings [2, 5–8]. In such macroscopic models, the calculated thermal parameters were used to predict the microstructure and the formation of any possible defects based on prior experience. Process maps plotting the occurrence of defects versus G and R have also been proposed as a performance criterion in process models [6, 7]. Other authors have suggested that these maps are not appropriate for the accurate prediction of grain defects in complex shaped large SX parts with abrupt changes in section size, since they were developed for castings with simple shapes (such as cylinders or plates) [8, 9].

More recently, Schneider *et al*. modeled micro- and macro-segregation and freckle formation in SX Ni-base superalloys by solving the macroscopic mass, momentum, energy, and species equations [10]. The formation of stray grains during directional solidification of a Ni-base superalloy was studied by modeling the movement and remelting of dendrite fragments [11]. Carter *et al*. have recently described a process model for grain selection during the solidification of SX superalloy castings which is based on heat transfer in the vicinity of the chill region and a cellular automaton analysis of the subsequent competitive growth of grains through a helix selector during directional solidification process. A tip-growth model has recently been presented to simulate the formation of low-angle boundaries in SX castings [12]. In this model, the tip velocity dependence on local undercooling is described by a power-law approximation of the tip velocity solution using the KGT model [13] and the dendritic structure is simulated by modeling the growth of the solid as a series of branching events.

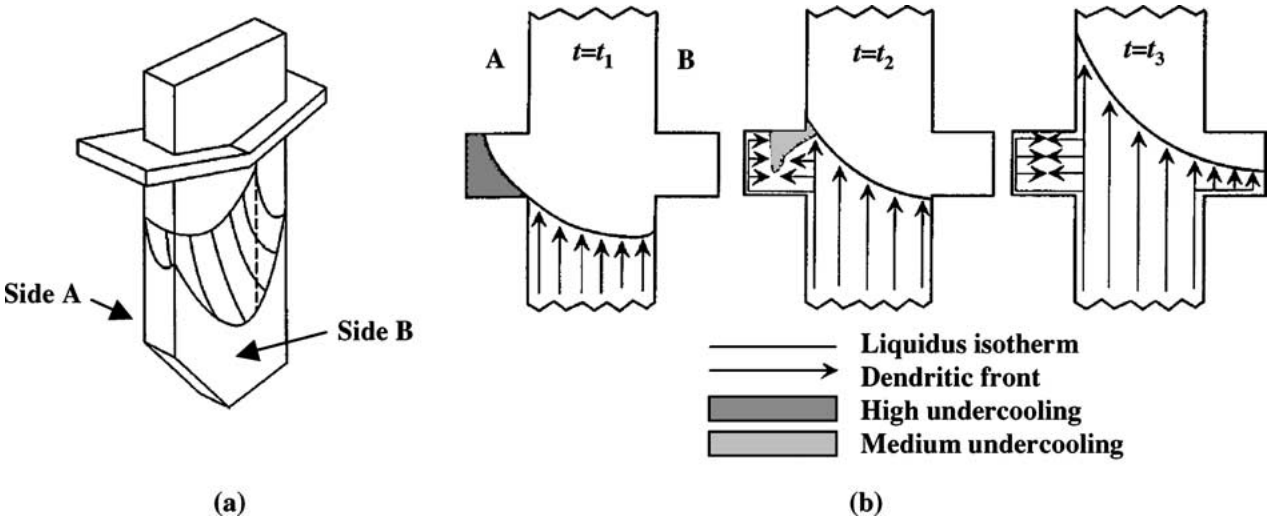

Figure 1 (a) Schematic of the isotherms estimated from the microstructure by Napolitano *et al*. for a SX blade cast in a cluster. (b) Schematic of the growth into the platform region, illustrating the difference in the dendritic patterns due to the effect of the platform geometry and the through-thickness gradient. Side A is outward facing, while side B is inward facing (after [12]).

It is known that some types of defects in SX parts are related to curvature of the liquidus isotherm while it is passing through enlargements in the cross section of the component (e.g., the platform of a turbine blade) [14]. This condition is exacerbated when several blades are cast in a cluster [12, 15]. Fig. 1a schematically depicts the liquidus isotherm plane in a turbine blade being cast as part of a cluster of blades [12]. The through-thickness thermal gradient can be seen from the outward facing side (side A) to the inward facing side (side B). It has already been observed that freckle channels tend to occur at the steepest regions of the solid-liquid interface, i.e., towards side A [15]. Indeed, this type of asymmetric concave upward solidification, interacting with the platform geometry, can result in increasing defects. The longitudinal section of the blade is shown in Fig. 1b. As the front approaches the platform, $t = t_1$, a significant degree of undercooling develops in the liquid within the platform on side A (i.e., dark gray region in Fig. 1b). As the front passes the mold corner, $t = t_2$, lateral growth of secondaries from the original primary dendrite into the platform is very fast due to the high undercooling (i.e., light gray region in Fig. 1b). This can generate a complex branching pattern of the dendritic structure, such as that at $t = t_3$. Alternatively, when there is sufficient undercooling, new grains may nucleate stray grain defects, which grow into the undercooled melt. On the inward side B of the casting, a quite different situation is observed. The undercooling in the platform is only that necessary to drive the motion of the dendrite tips. The front is free to follow the isotherm and is never constrained geometrically, as it is on side A. The result in this case should be a well-ordered dendritic structure. Clearly, it can be concluded that the probability of the formation of structural defects is largely dependent on the curvature of the solidification front, which in turn depends on the geometrical arrangement of the cluster. Prior models presented so far (e.g. [12]) have not been able to simulate the full dendritic microstructure in such conditions.

In this work a cellular automaton-finite difference (CAFD) model was extended to investigate the effect of changes in both the cross sectional area (i.e., geometrical discontinuities) and the shape of isotherms on dendrite growth during SX solidification of a binary approximation of a Ni-base superalloy. The dendritic structure formed in SX solidification when passing an increase in cross-sectional area was simulated with a range of different imposed isotherm shapes. The simulation results were compared with the experimental observations of Napolitano *et al*. [12].

2. Model theory

A two dimensional CAFD model, developed to simulate the solidification of aluminum and nickel alloys (described in detail previously [16–18]) was extended to simulate grid independent solute diffusion controlled growth of dendritic grains for the complex geometries. Both the CA and FD components of the model run on the same regular square grid and with the same time step. The spatial cells can be divided into two categories: "mold cells" and "alloy cells". Each "alloy cell" can have three states: liquid, solid and "growing" (i.e., a mixture of solid and liquid), while the "mold cells" are assigned a special flag to make them distinct from the others. Solute diffusion and grain growth are only performed in the alloy cells, and a zero-flux boundary condition is applied between alloy and mold cells.

Solute diffusion was calculated using an explicit finite difference method, and the changing rate of solid fraction (f_S) in a growing cell is determined jointly by solute diffusion and the variation of the concentration in that cell, expressed as:

$$C_L(1-k)\frac{\partial f_S}{\partial t} = -\nabla\cdot\{[(1-f_S)D_L + f_S k D_S]\nabla C_L\} + [1-(1-k)f_S]\frac{\partial C_L}{\partial t}, \quad (1)$$

where C_L is the solute concentration, k the partition coefficient, t time, and D_L and D_S diffusion coefficients in liquid and solid, respectively. The solute concentration (C_L) in the growing cells is calculated

by

$$C_{\mathrm{L}} = C_{\mathrm{L}}^{*} - \frac{1 - f_{\mathrm{S}}}{2} \Delta x G_{\mathrm{C}}, \tag{2}$$

where C_{L}^{*} is the equilibrium concentration at the solid/liquid interface, which can be obtained from the phase diagram at a given temperature, G_{C} the concentration gradient in front of the interface, and Δx the cell size.

The growth of solid and the effect of crystallographic anisotropy are accounted for by implementing an adaptation of the decentered square growth algorithm developed by Gandin *et al.* [19] to incorporate solute diffusion. The growth of the grain was represented by the successive growth of small squares associated with each cell, with the diagonals of each square oriented parallel to the crystallographic ⟨10⟩ directions of initial grain. The increase of the half diagonal dimension of the squares during a CA time step, ΔL, is related to the solid fraction by

$$\Delta L = \sqrt{2} \Delta x \cdot \Delta f_{\mathrm{S}}. \tag{3}$$

When a square grows large enough to touch any neighboring liquid cell, this cell is captured and a new square, growing from the point of contact with the new cell, is then associated with it. The new square is generated in such a way that it has the identical orientation of the old one, with one corner overlapping it, i.e., by shifting the center of the old square along one diagonal and reducing the size correspondingly.

3. Results and discussion

In order to demonstrate the effect of mold geometry on dendritic growth, the platform region of a turbine blade (Fig. 2) was chosen as the simulation domain. The domain is 5.5 mm wide and 8 mm high containing a mold wall with a thickness of 0.5 mm. The domain was then discretized using a regular grid of 5 μm square cells. A zero-flux boundary condition was applied at all boundaries. Different thermal conditions were applied in the simulations to investigate the effect of the temperature field on the growth pattern of dendrites.

Firstly, the thermal condition of horizontal isotherms with a temperature gradient of 12 K/mm moving upwards at a constant velocity of 150 μm/s was considered. The predicted dendritic structure and undercooling profiles at different times are shown in Fig. 2. A grain was placed at the bottom-right corner of the

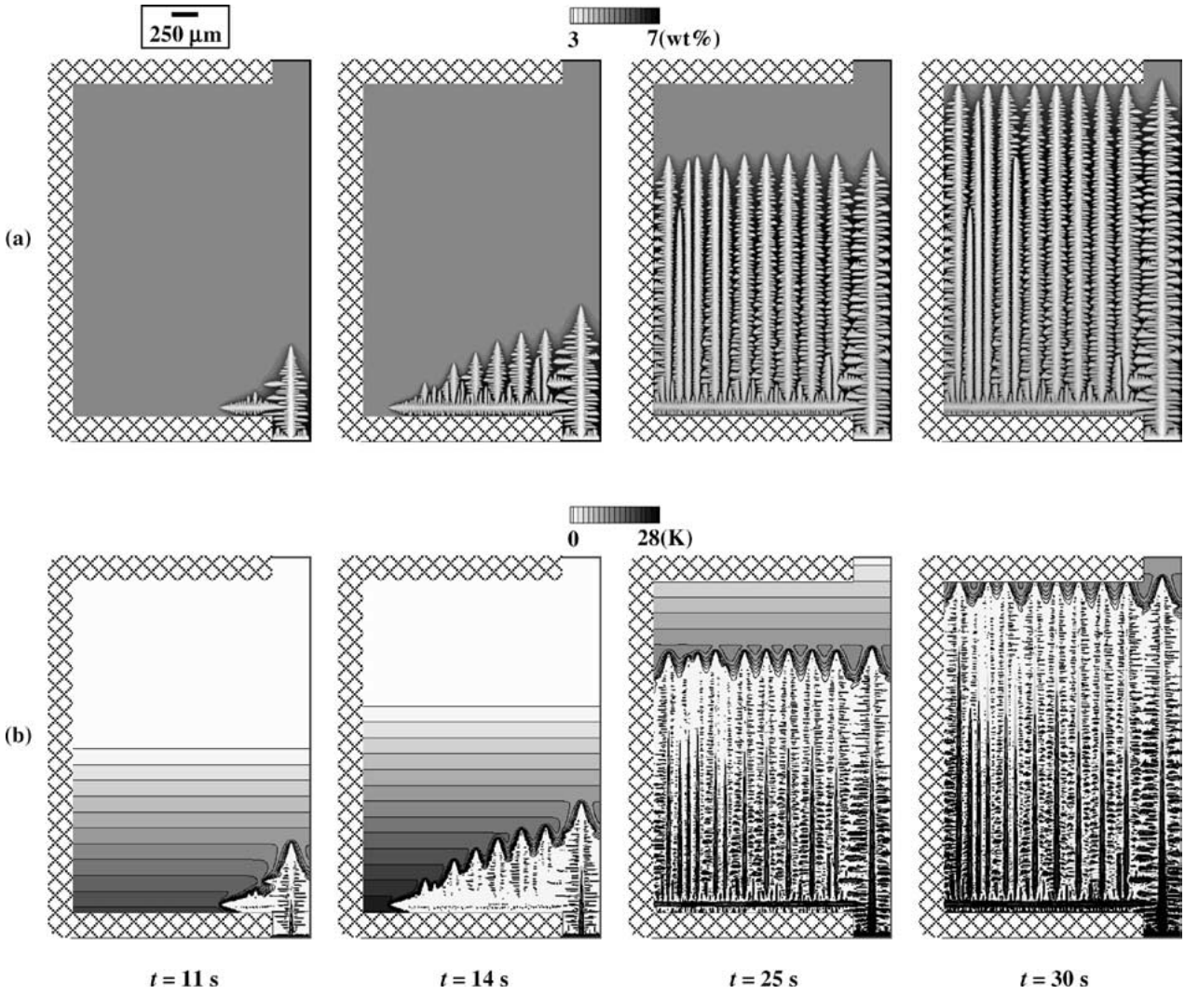

Figure 2 (a) Predicted dendritic structure and (b) solutal adjusted undercooling distribution under thermal conditions of horizontal isotherms moving at a constant velocity of 150 μm/s.

domain, with one of its ⟨10⟩ directions fully aligned with the vertical temperature gradient. After 11 s growth, the grain starts to propagate a secondary dendrite around the mold corner. A significant degree of undercooling develops in front of the secondary dendrite as macroscopic solidification proceeds vertically, reaching 20.7 K, which is about twice that in front of the original primary dendrite, 10.8 K. As a result of the high undercooling, the secondary dendrite grows at a much faster rate than the primary dendrite. After 14 s, the secondary dendrite approaches the outside vertical wall of the platform, with the tip undercooling having increased to 26.1 K. In the platform region, many tertiary dendrites emanate with a random initial spacing on both sides of the developing secondary dendrite. However, because of the constraint of the mold wall, only those facing upward can grow. The spacing between these new columnar dendrites is quickly reduced through an overgrowth mechanism. Although the tertiary dendrites near the outside wall are formed much later than those near the center, they grow much faster because of higher tip undercooling. The macroscopic solidification front rapidly approaches the shape of isotherms. Meanwhile, the degree of maximum undercooling decreases to approach that in front of the original primary dendrite. After 25 s, an almost flat front is achieved, and the maximum undercooling near the dendrite tips is reduced to 13.3 K, just marginally higher than the tip undercooling of primary dendrite, 11.4 K. Finally, a well-ordered dendritic structure is obtained at 30 s, when the solidification front passes the platform region, with all the tertiary dendrites terminating at the upper wall of platform. This simulation shows that, for horizontal isotherms, the abrupt change in the cross section of the mold results in a significant increase of undercooling in front of the lateral secondary dendrite near the lower wall of the platform. This can reach a value more than twice the tip undercooling of the primary dendrite, and if heterogeneous nuclei were present, there would be a much greater chance of stray grains forming. The tertiary dendrites emanating from the secondary grow rapidly, reducing the undercooling difference with the original primary, until the tertiary and primary dendrite tips become isothermal.

In the second example, the effect of the direction of the temperature gradient was investigated. As shown in Fig. 3b, the temperature gradient was inclined at 45° relative to the macroscopic solidification direction and the magnitude of the gradient was the same as in the previous case, 12 K/mm. Comparing Figs 2 and 3, it is

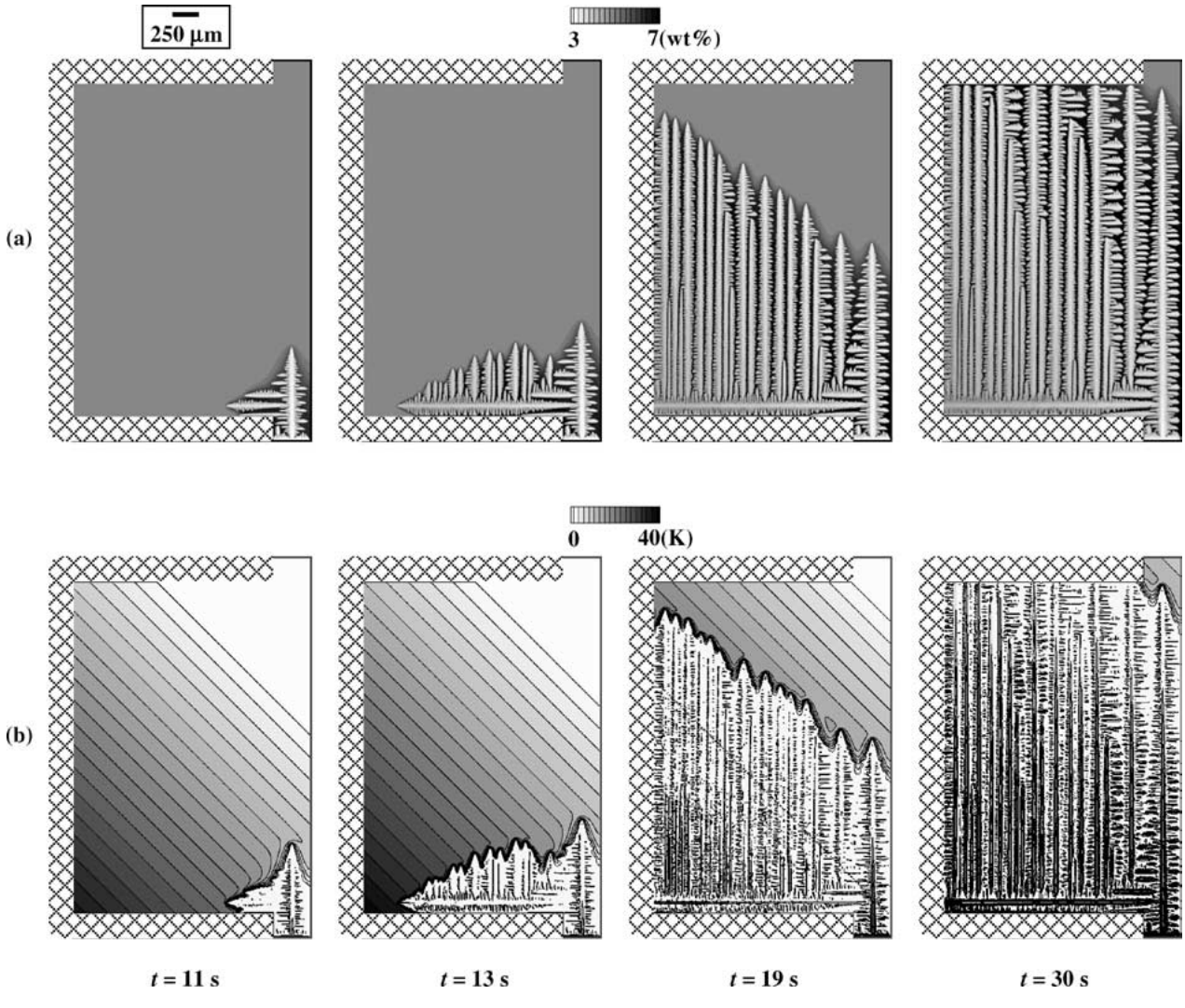

Figure 3 (a) Predicted dendritic structure and (b) solutal adjusted undercooling distribution under thermal conditions of 45° inclined isotherms in respect to the growth direction moving at a constant velocity of 150 μm/s.

found that at the early stage of growth, the development of the dendritic microstructure is (for $t \leq 15$ s) very similar. However, they diverge after ~15 s because of the effect of the inclined isotherms on the tip undercooling and growth. After 19 s of growth the solidification front approaches the 45° inclination of the isotherms (Fig. 3a, $t = 19$ s). Moreover, the fine dendritic structures also exhibit some differences. In Fig. 2a all the tertiary dendrites grow symmetrically, but in Fig. 3a, they develop asymmetrically, with more branches on the right hand side than the left hand side. Because of the inclination of the isotherms, an even higher undercooling develops as high as 39.6 K at the left-bottom corner, which is nearly four times that in front of the primary dendrite, 10.9 K. The propensity for stray grains to nucleate is even greater than with horizontal isotherms. The change in the direction of temperature gradient, can clearly affect both the macro- and micro-scale dendritic structures, as well as the maximum undercooling.

In the work of Napolitano *et al*. [12], they suggested that the true isotherm shape is concave (Fig. 1b). This shape was simulated using a polynomial function (Fig. 4). For the example shown, at the outside wall, the value of temperature gradient is about 20 K/mm, while at the center it is about 6 K/mm (with a mean temperature gradient of approximately 12 K/mm). The direction of the gradient relative to the vertical direction varies from 70° at edge to 0° at the center. Fig. 4b shows the undercooling ahead of the dendrites at different times, and the maximum undercooling in the corner reaches 44.4 K, a little more than four times higher than that ahead of the primary dendrite, 10.8 K. Fig. 4a shows the evolution of the dendritic structure, with the fastest growth direction marked out by a white arrow at each time. At an early stage (Fig. 4a, $t = 16.5$ s), the secondary dendrite grows very fast from right to left, until it reaches the outside wall of the platform. Thereafter, the upward tertiary dendrite near the outside wall reaches a maximum growth velocity, growing from the bottom to the top in 9 s. During the same time, the original primary dendrite only extends a distance one-fifth of that traversed by the fastest growing tertiary. As the tertiary dendrites approach the upper wall, they branch again. The small dendrites growing from left to right, block the growth of other relatively slow growing tertiary dendrites. However, eventually all these lateral branches are stopped by the original primary dendrite and a complex dendritic pattern is obtained, with a boundary between differently oriented dendrites, similar to a grain boundary, being formed. Fig. 5 compares

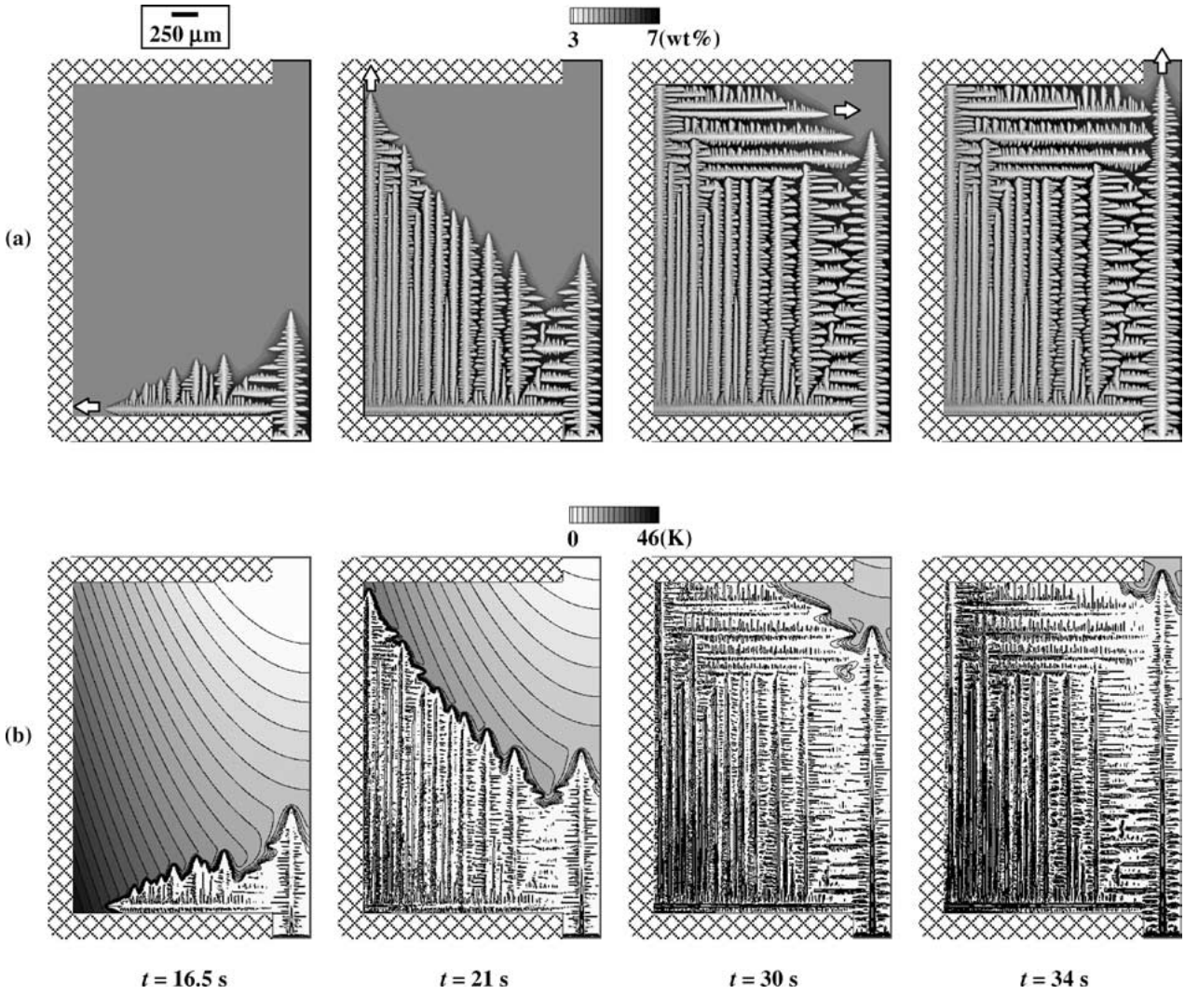

Figure 4 (a) Predicted dendritic structure and (b) solutal adjusted undercooling distribution under thermal conditions of concave isotherms, as suggested by Napolitano *et al*. [12], moving at a constant velocity of 150 μm/s.

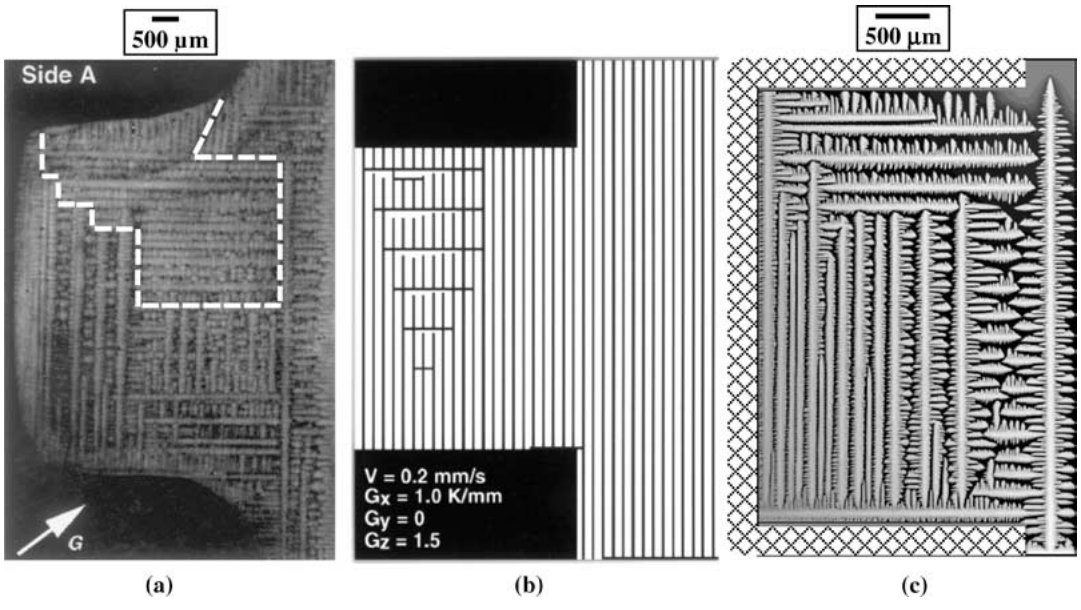

Figure 5 (a) Complex branching dendritic microstructure experimentally observed by Napolitano *et al*. at the outward facing platform section of a SX Ni-based superalloy blade (after [12]). (Note that the boundary between differently oriented dendrites is marked by a dashed line.) (b) The microstructure predicted by the tip-growth model of Napolitano *et al*. (after [12]). (c) The microstructure predicted by the present CAFD model.

the dendritic structure simulated in this study with the microstructure observed experimentally as well as the predicted dendritic structure by Napolitano *et al*. [12] in a Ni-based superalloy as discussed earlier. The boundary between the differently oriented dendrites is marked in the experimental micrograph by a dashed line. As can be seen, both models have correctly predicted the branching mechanism happening at the top of the platform region that results in a columnar array of dendrites perpendicular to the original primary dendrite. However, the model presented in this study simulates the full development of the unevenly spaced secondary/tertiary arms and the resultant changes in microsegregation between them by solving for solute diffusion. Although the current work gives a better prediction of the extent to which the perpendicular growth extends back into the core of the blade, a fully coupled macro-meso model calculation would have to be performed to determine if the model can capture more of the finer details.

In terms of the functionality of the SX components, the occurrence of these complex self-convergent dendritic structures should be avoided, both in terms ensuring consistent properties and because the huge undercoolings occurring increases the chance of stray grains forming. Application of these mesomodels should allow the operating parameters of the SX system to be adjusted so that a well-ordered uniform columnar dendritic structure is achieved throughout the entire component.

4. Conclusions

A combined CAFD model of solute diffusion controlled dendritic solidification was developed and applied to simulate the solidification in a geometry approximating the platform region of a SX turbine blade. Different shapes of isotherms moving at a constant velocity were applied. It was found that a significant degree of undercooling develops at the platform region in front of the secondary dendrites, and the maximum undercooling increases as the local temperature gradient increasingly deviates from the withdrawal direction. The increase in undercooling for the curved interfaces observed when casting clusters of blades is nearly four times the steady state value, with a significant increase in the chance of stray grains forming. Even if stray grains are avoided, a complex dendritic pattern with a self-convergent grain boundary forms in excellent agreement with experimental observations.

Acknowledgements

The authors would like to thank the EPSRC (grant GR/N14132) for financial support and their collaborators (Special Metals Wiggin Ltd., Rolls-Royce plc, Wyman-Gordon Ltd and QinetiQ) for their assistance and the provision of both materials and information.

References

1. M. MCLEAN, in "Directionally Solidified Materials for High Temperature Service" (The Metals Society, 1983) p. 5.
2. M. MEYER TER VEHN, D. DEDECKE, U. PAUL and P. R. SAHM, in Proceedings of the Superalloys 1996, Pennsylvania, USA, edited by R. D. Kissingger, D. J. Deye, D. L. Anton, A. D. Cetel, M. V. Nathal, T. M. Pollock and D. A. Woodford (TMS, 1996) p. 471.
3. R. J. SCHAEFER, D. R. BLACK, M. D. VAUDIN, B. R. MUELLER and A. F. GIAMEI, in Proceedings of the 4th Decenninal International Conference on Solidification Processing, Sheffield, UK, edited by J. Beech and H. Jones (Sheffield, UK, 1997) p. 37.
4. N. D'SOUZA, M. G. ARDAKANI, M. MCLEAN and B. A. SHOLLOCK, *Metall. Mater. Trans.* A **31A** (2000) 2877.
5. K. O. YU, M. J. BEFFEL, M. ROBINSON, D. D. GOETTSCH, B. G. THOMAS, D. PINELLA and R. G. CARLSON, *Trans. AFS* (1990) 417.
6. T. M. POLLOCK, W. H. MURPHY, E. H. GOLDMAN, D. L. URAM and J. S. TU, in Proceedings of the Superalloys 1992, Champion, PA, Sept. 20–24, edited by S. D. Antolovich, *et al.* (TMS, 1992) p. 125.

7. K. O. YU, J. J. NICHOLAS and M. ROBINSON, *JOM* **44** (1992) 21.
8. A. L. PURVIS, C. R. HANSLITS and R. S. DIEHM, *ibid*, **46** (1994) 38.
9. A. L. PURVIS and C. R. HANSLITS, in Proceedings of the Modeling of Casting, Welding and Advanced Solidification Processes VII, London, UK, edited by M. Cross and J. Campbell (TMS/AIME, 1995) p. 475.
10. M. C. SCHNEIDER, J. P. GU, C. BECKERMANN, W. J. BOETTINGER and U. R. KATTNER, *Metall. Mater. Trans.* A **28A** (1997) 1517.
11. J. P. GU, C. BECKERMANN and A. F. GIAMEI, *ibid*. **28A** (1997) 1533.
12. R. E. NAPOLITANO and R. J. SCHAEFER, *J. Mater. Sci*. **35** (2000) 1641.
13. W. KURZ, B. GIOVANOLA and R. TRIVEDI, *Acta Metall.* **34** (1986) 823.
14. U. PAUL, P. R. SAHM and D. GOLDSCHMIDT, *Mat. Sci. and Eng.* A **A173** (1993) 49.
15. S. M. COPLEY, A. F. GIAMEI, S. M. JOHNSON and M. F. HORNBECKER, *Metall. Trans*. A **A1** (1970) 2193.
16. P. D. LEE, D. SEE and R. C. ATWOOD, in Proceedings of the Cutting Edge of Computer Simulation of Solidification and Casting, Osaka, Japan, Nov. 14–16, 1999, edited by I. Ohnaka and H. Yasuda (ISIJ, 1999) p. 97.
17. W. WANG, A. KERMANPUR, P. D. LEE, M. MCLEAN, X. WANG, R. M. WARD and M. H. JACOBS, in Proceedings of the International Symposium on Liquid Metal Processing and Casting, Santa Fe, New Mexico, Sept. 23–26, 2001, edited by A. Mitchell and J. Van Den Avyle (AVS, NY, 2001) p. 267.
18. W. WANG, A. KERMANPUR, P. D. LEE and M. MCLEAN, *Int. J. Cast Metals Research* **15** (2002) 269.
19. C. A. GANDIN and M. RAPPAZ, *Acta Mater*. **45** (1997) 2187.

Received 22 January
and accepted 22 July 2003